

Exoskeleton-Assisted Balance and Task Evaluation During Quiet Stance and Kneeling in Construction

Gayatri Sreenivasan, Chunchu Zhu, and Jingang Yi

Abstract—Construction workers exert intense physical effort and experience serious safety and health risks in hazardous working environments. Quiet stance and kneeling are among the most common postures performed by construction workers during their daily work. This paper analyzes lower-limb joint influence on neural balance control strategies using the frequency behavior of the intersection point of ground reaction forces. To evaluate the impact of elevation and wearable knee exoskeletons on postural balance and welding task performance, we design and integrate virtual- and mixed-reality (VR/MR) to simulate elevated environments and welding tasks. A linear quadratic regulator-controlled triple- and double-link inverted pendulum model is used for balance strategy quantification in quiet stance and kneeling, respectively. Extensive multi-subject experiments are conducted to evaluate the usability of occupational exoskeletons in destabilizing construction environments. The quantified balance strategies capture the significance of knee joint during balance control of quiet stance and kneeling gaits. Results show that center of pressure sway area reduced up to 62% in quiet stance and 39% in kneeling for subjects tested in high-elevation VR/MR worksites when provided knee exoskeleton assistance. The comprehensive balance and multitask evaluation methodology developed aims to reveal exoskeleton design considerations to mitigate the fall risk in construction.

Note to Practitioners—Construction workers commonly perform tasks that require prolonged quiet stance or kneeling gaits on high elevations. Worker balance can be undermined by chronic knee injuries, musculoskeletal disorders and destabilizing visual perturbations caused by occupational activities. Wearable knee exoskeletons have evolved as promising interventions to reduce knee joint stress across a variety of work gaits in construction. Emerging technologies such as virtual- and mixed-reality (VR/MR) provide a platform to study underlying balance strategies workers employ to complete tasks when confronted by dynamic environment. The VR/MR-generated immersive elevated welding work sites in this study are leveraged to examine the effects of threatening visual stimuli, wearable exoskeletons and construction tasks on worker balance and performance. Intersection point height frequency analysis is used to observe and quantify the chosen neural balance strategy during various testing scenarios. Emphasis is placed on exploring the often-neglected role of the knee joint to facilitate research on knee-based balance augmenting exoskeleton controllers that can support subtle gaits like quiet

stance and kneeling. The experimental results provide insight into the efficacy of knee exoskeletons in improving construction worker stability and task performance. The results highlight the need for a holistic approach to exoskeleton design and evaluation to ensure that developed solutions can be safely and successfully integrated into the workplace environment.

Index Terms—Postural balance, knee exoskeleton, virtual/mixed reality, automation in construction, biomechanics

I. INTRODUCTION

Construction workers commonly perform tasks that require prolonged quiet stance or kneeling gaits on high elevations or cluttered environments. These awkward gaits in construction increase the risk of work-related musculoskeletal disorders (WMSDs), such as knee pain or knee osteoarthritis [1]. In both stance and kneeling gaits, human workers are inherently unstable in an upright posture, requiring continuous engagement of muscles to regulate joint torques and maintain postural stability [2], [3]. Although the neural balance mechanism at quiet stance has been extensively studied, the underlying control strategy remains elusive [4]. Previous studies have investigated the ankle or hip strategies during quiet standing [5], [6], and most of them used the single-link inverted pendulum model to analyze human balance strategies. The importance of the knee and hip joints at quiet stance was demonstrated in [7], [8]. However, the knee joint contribution to maintaining an upright stance is often overlooked. Few research work was reported for postural control of kneeling gaits. In [9], a comparative analysis of quiet kneeling and stance postures was conducted with a focus on the role of visual feedback during kneeling. A single inverted pendulum model was used in [6] to study the influences of elevation on the postural balance of kneeling gait.

All of the works above primarily use the motion of the body's center of mass (COM) or center of pressure (COP) to quantify the human balance performance. Metrics such as power spectral density (PSD) of the COP and acceleration were used to compare and discriminate between quiet stance and kneeling [6], [9]. The metrics solely derived from COP or COM are limited in capturing the balance dynamics and control as they are unable to account for both translational and rotational body accelerations. To address these limitations, the study in [4], [10] introduced the intersection point (IP) of the ground reaction forces (GRF) during quiet stance. In [11], a double-inverted pendulum (DIP) model was leveraged to quantify the frequency-dependence of the IP height during quiet stance. The study focused on quantifying ankle and hip

The work of Jingang Yi was supported by US NSF under Award CMMI-2222880 and the work of Gayatri Sreenivasan was supported by US NSF under Award DGE-2021628. An earlier version of this paper was presented in part at the 2023 IEEE International Conference on Automation Science and Engineering, Auckland, New Zealand, August 26-30, 2023 [DOI: 10.1109/CASE56687.2023.10260384]. (*Corresponding author: Jingang Yi*)

G. Sreenivasan was with the Department of Electrical and Computer Engineering, Rutgers University, Piscataway, NJ 08854 USA. She is now with Elmore Family School of Electrical and Computer Engineering, Purdue University, West Lafayette, IN 47907 USA (email: gs912@scarletmail.rutgers.edu).

C. Zhu and J. Yi are with the Department of Mechanical and Aerospace Engineering, Rutgers University, Piscataway, NJ 08854 USA (email: chunchu.zhu@rutgers.edu; jgyi@rutgers.edu).

joint strategies and emphasized the importance of multiple joint-level contributions to overall balance control.

Among the diverse environmental factors affecting balance control for construction workers, elevation is notably significant [12]–[14]. Acrophobia exacerbates this challenge, as it leads individuals to overestimate heights, intensifying fear and triggering physiological reactions that undermine balance [15]. Additionally, visual and environmental perturbations further compromise postural stability [16]. To address these challenges, wearable devices like knee exoskeletons have emerged as pivotal fall risk interventions [17]–[20]. However, little work has been done on knee-based balance augmentation for quiet stance and kneeling. Virtual- and mixed-reality (VR/MR) has been used to simulate high-elevation conditions and study neural balance control among construction workers [6], [21]. The work in [22] showed safety reinforcement training on construction workers’ fall risks using VR scenes. The work in [23] conducted neurophysiological assessments for welding task performance at virtual height to study cognitive effects on balance. A comprehensive review of VR/MR applications in construction safety can be found in [24].

The goal of this study is to investigate the influence of lower-limb joints, particularly the knee joint, on neural balance control in quiet stance and kneeling gaits. We also evaluate the impact of elevation and wearable knee exoskeletons on postural balance and welding task performance. Similar to previous studies (e.g., [11], [25], [26]), a linear quadratic regulator (LQR) is used as the human neural balance controller. The triple- and double-link inverted pendulum (TIP and DIP) models are built to capture the joint-level effects for quiet stance and kneeling gaits, respectively. The models are used to quantify the observed neural balance control strategy from frequency characteristics of the IP heights. The LQR allows for the explicit consideration of different parameters on balance performance, facilitating the interpretation of results in terms of physiological and biomechanical implications [11]. Human subject experiments are conducted using incorporating VR/MR environments that simulate realistic welding worksites at varying elevations to evaluate the influence of elevation on postural balance and task performance. The subjects are outfitted with a wearable knee exoskeleton to test the usability and functionality of the intervention. The combination of experimental data and model analysis helps the extraction of physiologically plausible insights into the balance strategy chosen by subjects. Both objective metrics and human subjective feedback confirm that the exoskeletons have the potential to improve both balance and task execution efficiency in construction.

The main contributions of this work are twofold. First, the study introduces new modeling and analysis for neural balance control that accounts for knee joint strategy with the IP height as the performance metric for quiet stance and kneeling. To the authors’ best knowledge, no previously reported work elucidates the involvement of knee joint strategy in quiet stance or kneeling gaits. Second, this study introduces a novel exploration of how elevation and the use of

wearable exoskeletons impact neural balance control during quiet stance and kneeling. The quantitative findings offer valuable insights for the development of balance-enhancing wearable robotic interventions. Compared with the previous conference presentation [27] that focused only on quiet stance, this work extends to kneeling gaits by introducing the DIP model to investigate the joint-level effects on postural balance control. Additionally, the VR/MR simulating welding tasks to assess worker performance is newly developed.

The rest of the paper is organized as follows. We introduce the multi-link models and neural balance control in Section II. The experimental setup and protocols are detailed in Section III. Data analysis and simulation pipelines are explained in Section IV. Section V presents the experimental and simulation results, followed by discussions in Section VI. Finally, we give the concluding summary in Section VII.

II. MULTI-LINK MODELS AND BALANCE CONTROL

In this section, we first present the inverted pendulum models that describe quiet stance and kneeling, respectively. Next, the IP for human postural balance is discussed followed by presentation of the LQR-based neural controller.

A. Biomechanical Models for Stance and Kneeling

Fig. 1(a) illustrates the welder’s stance posture and schematic consisting of three interconnected segments. The upper segment, which includes the head, arms, and trunk, is connected to the middle segment, representing the thigh, and the lower segment, representing the shank. In this study, only motion in the sagittal plane is considered. Fig. 1(b) shows the welder’s working pose when kneeling on the ground with both legs alongside the schematic of the DIP model. In the case of quiet stance, the ankle joint is assumed to be the pin joint on the ground, whereas for kneeling, the knee joint is assumed to be the pin joint on the ground and feet are assumed to support no weights. The joint angles and joint torques at the ankle, knee, and hip are denoted as θ_i and τ_i , $i = 1, 2, 3$, respectively. The masses and mass moments of inertia about the centers of each link are denoted as m_i and I_i , $i = 1, 2, 3$, respectively. The distance between the mass center and the lower end of each link is denoted as l_{c_i} , $i = 1, 2, 3$, respectively.

Defining $\theta_t = [\theta_1 \ \theta_2 \ \theta_3]^T$ and $\theta_d = [\theta_2 \ \theta_3]^T$, the equations of motion for the TIP/DIP models are written as

$$M_i(\theta_i)\ddot{\theta}_i + C_i(\theta_i, \dot{\theta}_i)\dot{\theta}_i + G_i(\theta_i) = \tau_i, \quad i = t, d, \quad (1)$$

where $M_i(\theta_i)$, $C_i(\theta_i, \dot{\theta}_i)$, and $G_i(\theta_i)$ are the inertia, Coriolis, gravitational matrices, and subscripts “t” and “d” for the TIP and DIP models, respectively. The details of these matrices are given in [28]. The human neural joint torques τ_i are given as

$$\tau_i = \tau_i^s + \mathbf{w}_i, \quad i = t, d,$$

where $\tau_t^s = [\tau_1 \ \tau_2 \ \tau_3]^T$ and $\tau_d^s = [\tau_2 \ \tau_3]^T$, $\mathbf{w}_i \sim \mathcal{N}(\mathbf{0}, \sigma_i)$ are the joint torque perturbations that are modeled as independently white Gaussian noises with zero mean and variance $\sigma_t = \text{diag}(\sigma_1^2, \sigma_2^2, \sigma_3^2)$ and $\sigma_d = \text{diag}(\sigma_2^2, \sigma_3^2)$.

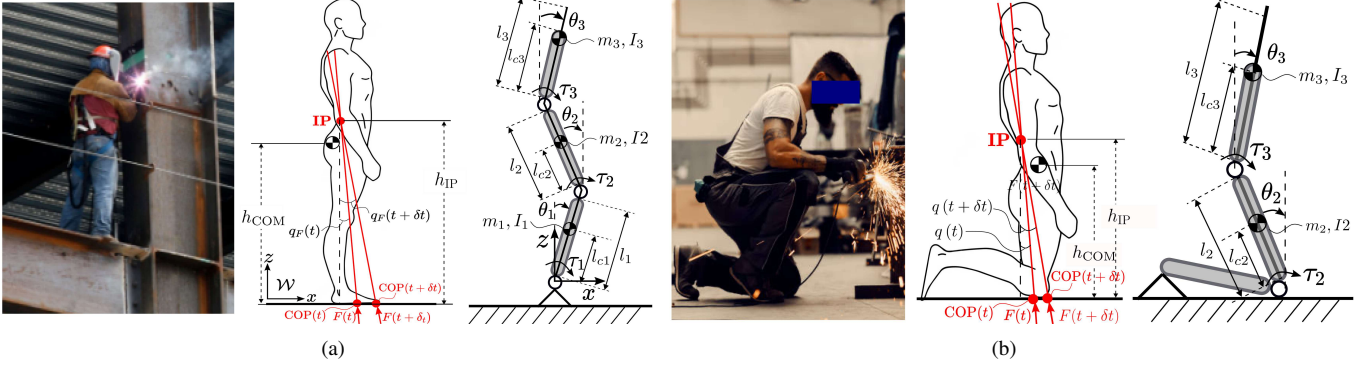


Fig. 1. Stance and kneeling gaits in construction. (a) From left to right: Welder stands while conducting welding task; schematic of COM and IP in stance; schematic of the TIP model. (b) From left to right: welder kneels on both legs; schematic of the COM and IP in kneeling gait; schematic of the DIP model.

Defining $x_i = [\theta_i^T \dot{\theta}_i^T]^T$, $i = t, d$, from (1), we obtain

$$\dot{x}_i = \begin{bmatrix} \dot{\theta}_i \\ M_i^{-1}(\theta_i) (\tau_i - C_i(\theta_i, \dot{\theta}_i) - G_i(\theta_i)) \end{bmatrix}. \quad (2)$$

The position vectors of the COM are denoted as $r_i^M = [x_i^m z_i^m]^T$, $i = t, d$, for stance and kneeling gaits, respectively. For stance posture, $x_t^m = -l_{c1} s_{\theta_1} - l_{c2} s_{\theta_1 + \theta_2} - l_{c3} s_{\theta_1 + \theta_2 + \theta_3}$ and $z_t^m = l_{c1} c_{\theta_1} + l_{c2} c_{\theta_1 + \theta_2} + l_{c3} c_{\theta_1 + \theta_2 + \theta_3}$, where notations $s_{\theta_i} = \sin \theta_i$, $c_{\theta_i} = \cos \theta_i$ for θ_i , and $s_{\theta_i + \theta_j} = \sin(\theta_i + \theta_j)$ for angles θ_i and θ_j , $i \neq j$, $i, j = 1, 2, 3$. For quiet stance, we define the Jacobian matrix of the COM to x_i as $J_t^M = -[J_t^{M1} J_t^{M2} J_t^{M3}]$, where $J_t^{M1} = r_t^M$, $J_t^{M3} = [l_{c3} c_{\theta_1 + \theta_2 + \theta_3} \quad l_{c3} s_{\theta_1 + \theta_2 + \theta_3}]^T$, and

$$J_t^{M2} = \begin{bmatrix} l_{c2} c_{\theta_1 + \theta_2} + l_{c3} c_{\theta_1 + \theta_2 + \theta_3} \\ l_{c2} s_{\theta_1 + \theta_2} + l_{c3} s_{\theta_1 + \theta_2 + \theta_3} \end{bmatrix}.$$

For kneeling gait, $x_d^m = -l_{c2} s_{\theta_2} - l_{c3} s_{\theta_2 + \theta_3}$ and $z_d^m = l_{c2} c_{\theta_2} + l_{c3} c_{\theta_2 + \theta_3}$. The Jacobian matrix of the COM is $J_d^M = -[J_d^{M2} J_d^{M3}]$, where $J_d^{M3} = [l_{c3} c_{\theta_2 + \theta_3} \quad l_{c3} s_{\theta_2 + \theta_3}]^T$ and

$$J_d^{M2} = \begin{bmatrix} l_{c2} c_{\theta_2} + l_{c3} c_{\theta_2 + \theta_3} \\ l_{c2} s_{\theta_2} + l_{c3} s_{\theta_2 + \theta_3} \end{bmatrix}.$$

In the above model for quiet stance, $l_{ci} = \frac{\frac{1}{2} m_i l_i + \sum_{j=i+1}^3 m_j l_j}{m_i}$, $i = 1, 2, 3$, and $m_t^t = m_1 + m_2 + m_3$. For kneeling gait, $l_{ci} = \frac{\frac{1}{2} m_i l_i + \sum_{j=i+1}^3 m_j l_j}{m_i}$, $i = 2, 3$, $m_d^t = m_2 + m_3$. The acceleration of the COM is obtained as $\ddot{r}_i^M = [J_i^M J_i^M] \dot{x}_i = \mathcal{J}_i^M \dot{x}_i$, where $\mathcal{J}_i^M = [J_i^M J_i^M]$, $i = t, d$. The GRFs in the horizontal and vertical directions are respectively computed as

$$F_i^x = m_i^t \ddot{x}_i^m, \quad F_i^z = m_i^t (\ddot{z}_i^m + g), \quad i = t, d, \quad (3)$$

where $g = 9.8 \text{ m/s}^2$ is the gravitational constant,

B. Intersection Point

The IP is the point in space where the net GRF vectors at adjacent time steps intersect. Fig. 1 illustrates the IP concept for quiet stance and kneeling. Unlike the COP or COM, the use of the IP takes into account the translational and angular

accelerations of the body and the IP height is used to quantify the neuromuscular control strategy.

The IP height, denoted by h_{IP} , is calculated using the COP and GRF data obtained from force plate measurements. The angle between the GRF vector and the vertical direction is denoted as $q(t)$ at time t ; see Fig. 1. Assuming subtle movements of the body and using a small angle approximation, we obtain

$$q(t) \approx \tan(q(t)) = \frac{F_x(t)}{F_z(t)}, \quad (4)$$

where $F(t) = [F_x(t) F_z(t)]^T$ is the GRF vector at t . It is clear that the relation between unfiltered $q(t)$ and COP is not linear. To calculate h_{IP} , we consider the COP position along the x -direction, denoted by $x_{CP}(t)$, at time moments of t and $t + \delta t$. From Fig. 1, we obtain

$$q(t) = \frac{x_{CP}(t)}{h_{IP}(t)}, \quad q(t + \delta t) = \frac{x_{CP}(t + \delta t)}{h_{IP}(t)}. \quad (5)$$

We solve for $h_{IP}(t)$ from (5) and obtain

$$h_{IP}(t) = \frac{x_{CP}(t + \delta t) - x_{CP}(t)}{q(t) - q(t + \delta t)}. \quad (6)$$

We will further discuss how to process $h_{IP}(t)$ in frequency domain to analyze the balance performance in Section IV.

C. Neural Balance Control

We linearize (2) around the upright equilibrium, that is, $x_i^e = \mathbf{0}$ under input $\tau_i^e = \mathbf{0}$, and obtain the linearized system

$$\dot{\bar{x}}_i = A_i^l \bar{x}_i + B_i^l \bar{\tau}_i^s + B_i^l w_i, \quad i = t, d, \quad (7)$$

where $\bar{x}_i = x_i - x_i^e$, $\bar{\tau}_i^s = \tau_i^s - \tau_i^e$, and A_i^l and B_i^l are the state and input matrices, respectively. The cost function is given as

$$J_i = \int_0^\infty [\bar{x}_i^T Q_i \bar{x}_i + (\bar{\tau}_i^s)^T R_i \bar{\tau}_i^s] dt, \quad (8)$$

where positive symmetric definite matrices Q_i and R_i penalize the state and control input, respectively. The solution to (8) is $\tau_i^s = -K_i^L x_i$, where K_i^L is the gain matrix that is solved by the Riccati equation. Matrix R_i , $i = t, d$, is

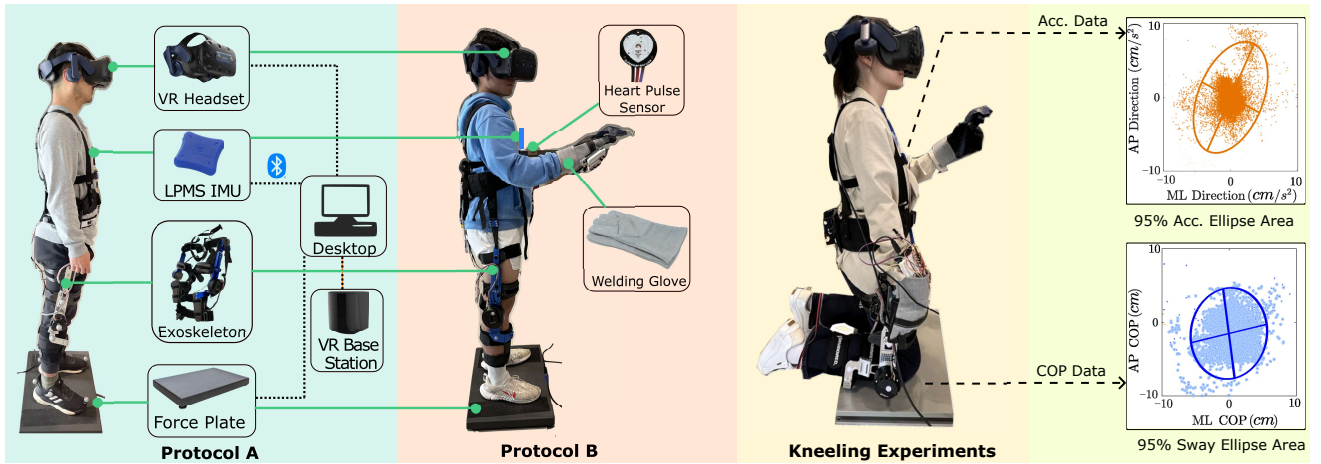


Fig. 2. The VR/MR-enhanced human subject balance experiment setup with wearable knee exoskeletons for Protocols A (left) and B (mid), and an explanation for the kneeling experiments and the 95% acceleration and sway ellipse area(right).

selected and designed as

$$\mathbf{R}_i = \alpha_i \beta_i, \quad (9)$$

where α_i is the parameter related to overall control effort, and β_i describes the relative magnitude of joint efforts. Here $\beta_t = \text{diag}(\beta_1, \beta_2, \beta_3)$ for the stance controller, and $\beta_d = \text{diag}(\beta_2, \beta_3)$ for the kneeling controller. β_1 , β_2 , and β_3 represent effort at the ankle, knee, and hip joints, respectively. The LQR neural control guarantees stability if $(\mathbf{A}_i^l, \mathbf{B}_i^l)$ is controllable, and \mathbf{Q}_i is chosen as an identity matrix to equally penalize each state's deviation.

Following observations from [11], we obtain the physiological meaning of three sets of parameters (i.e., α_i , β_i , σ_i) that are associated with the LQR-based neural controller: (i) α_i characterizes the control effort employed to attain stability, (ii) β_i penalizes the contribution of ankle, knee, and hip joints control, and (iii) σ_i signifies the neuromuscular impedance and noise at each joint. The output of (7) is considered as $y_{1i} = -F_i^x$, $i = t, d$, and $y_{2t} = \tau_1$ (ankle torque for stance) or $y_{2d} = \tau_2$ (knee torque for kneeling) that are directly measured from force plate. The negative sign in y_{1i} is due to the convention that a positive horizontal GRF is directed towards the positive x -axis; see Fig. 1(a). From (3) and using the Jacobian matrix, we obtain

$$y_{1i} = -m_i^t \dot{x}_i^m = -m_i^t [1 \ 0] \mathcal{J}_i^M \dot{\mathbf{x}}_i = \mathbf{C}_i \mathbf{x}_i + \mathbf{D}_i^1 \tau_i^s,$$

where $\mathbf{C}_i = -m_i^t [1 \ 0] \mathcal{J}_i^M \mathbf{A}_i^l$ and $\mathbf{D}_i^1 = -m_i^t [1 \ 0] \mathcal{J}_i^M \mathbf{B}_i^l$. It is clear that $y_{2i} = \mathbf{D}_{2i} \tau_i^s$, where $\mathbf{D}_{2i} = [1 \ 0_i]$, $i = t, d$, and $\mathbf{0}_t = [0 \ 0]$ and $\mathbf{0}_d = 0$. Therefore, output equation is

$$\mathbf{y}_i = \begin{bmatrix} y_{1i} \\ y_{2i} \end{bmatrix} = \begin{bmatrix} \mathbf{C}_i \\ \mathbf{0} \end{bmatrix} \mathbf{x}_i + \begin{bmatrix} \mathbf{D}_{1i} \\ \mathbf{D}_{2i} \end{bmatrix} \tau_i^s, \quad i = t, d.$$

III. EXPERIMENTS

A. Experiment Setup and Protocol

Fig. 2 shows the experimental setup for quiet stance and kneeling gaits in construction. A wearable inertial measurement unit (IMU) (from LP-RESEARCH Inc.) was attached

to the subject's chest to measure postural sway accelerations. A force plate (from Bertec Corporation) was used to collect GRF and COP data. An extra pulse sensor was used to capture the subject's heart rate during experiments. The human subjects were also equipped with a bilateral knee exoskeleton with quasi-direct drive actuators. The exoskeleton possessed high-torque, high-backdrivability, and high-bandwidth features [29]. The design was compact and light-weight (unilateral unit weighed only 1.7 kg, including electronics and battery) with high-torque output (35 Nm peak torque), large range of motion (0-160 deg flexion), and high rotation speed (16.2 rad/s). All sensor data were synchronized and collected at 100 Hz on a portable high-performance micro-processor (Intel NUC7i7DNK, Intel Corp.).

A VR system (HTC Vive Pro) was employed to immerse the subjects in diverse visual environments during test trials. A virtual construction site was built with the Unity game engine to simulate the typical low-elevation (LE) and high-elevation (HE) construction work environments. Fig. 3(a) shows the VR viewpoint for the quiet stance and Fig. 3(b) shows the VR scene for welding task. The LE scenario depicted the subject standing on a small platform slightly elevated from the ground. The HE scenario on the other hand simulated the subject standing atop a 30-story building under ongoing construction.

Eleven able-bodied human subjects (4 females, 7 males, weight: 67 ± 10 kg, height: 170 ± 8 cm, age: 25 ± 2.5 years) were recruited in the study. All participants provided informed consent and self-reported being in good health. The experimental protocol was approved by the Institutional Review Board (IRB) at Rutgers University. This study's experimental protocol encompasses two gait situations: quiet stance and kneeling. Each gait experiment is subdivided into two protocols, labeled Protocols A and B. The subjects were labeled from S1 to S11. The stance experiments involved the participation of 2 female and 5 male subjects, while the kneeling experiments were conducted with a group of 2 female and 4 male subjects. Subjects S6 and S7 participated in both stance and kneeling experiments.

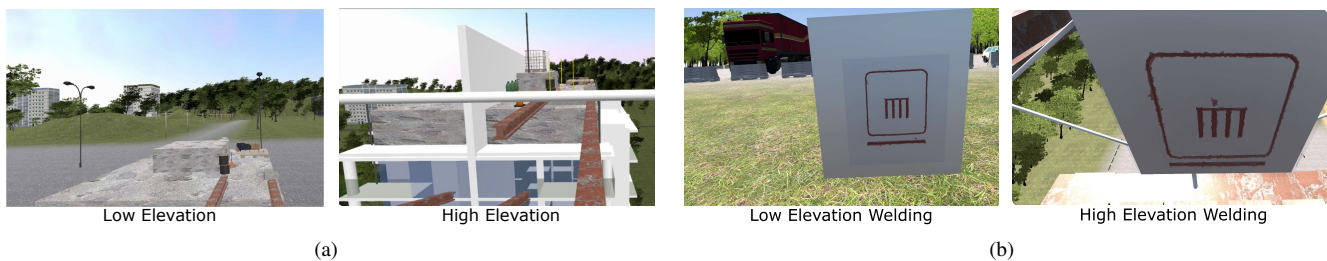


Fig. 3. (a) VR scene in Unity engine at LE (left) and HE (right) views. (b) VR view in the welding tasks at LE ground view (left) and HE view (right).

1) *Protocol A - Posture balance evaluation*: Subjects were asked to perform a quiet stance and kneeling task while maintaining balance in a simulated environment for 60 s. The visual stimuli varied between trials by altering the LE and HE. This setup facilitated two distinct trials, each designed to assess the impact of elevation perception on balance. The wearable knee exoskeleton was introduced in a subsequent variation.

The research work in [30] has shown that the knee joint's deviation from a natural stance is small and a stiffness-based controller effectively reduces muscle fatigue and enhances balance. Consequently, a stiffness knee torque controller $\tau_e = -k_r\theta_2$ is used for the quiet stance gait, where τ_e is the exoskeleton output torque, k_r represents the reference joint stiffness, and θ_2 denotes the knee joint's deviation from a natural stance. In contrast, during kneeling, the knee joint acts as a pin joint, bearing a significant portion of the body's weight. This increased loading on the knee joint leads to large variations in joint angles and requires great effort to maintain balance. Inspired by the work in [31], the inertia and Coriolis terms in (1) are neglected and a proportional-derivative (PD) knee assistive torque controller with gravity compensation is considered

$$\tau_e = -k_p\theta_2 - k_d\dot{\theta}_2 - \gamma g \left[\frac{m_3}{2} (l_2 s\theta_2 - l_{c3} s\theta_3) + m_2 l_{c2} s\theta_2 \right],$$

where k_p and k_d are the proportional and derivative gains, respectively, and $\gamma \in (0, 1)$ is the assistance weight factor.

Subjects were required to complete four trials in Protocol A. The trials, termed test of interest (TOI), incorporated both elevation scenarios with and without the exoskeleton support: (i) TOI 1: LE without the exoskeleton; (ii) TOI 2: HE without the exoskeleton; (iii) TOI 3: LE with the exoskeleton; and (iv) TOI 4: HE with the exoskeleton. A five-min rest period was given between each trial to minimize fatigue and ensure consistent performance.

2) *Protocol B - Welding task assessment*: A welding trade was considered as welders often have to hold awkward gaits while conducting tasks with precision requirements. The dual task of maintaining upright balance and performing welding accurately is challenging. Protocol B introduced a welding task in the VR scene, see Fig. 3(b), simulating a dynamic and task-focused assessment. As shown in Fig. 2, participants were equipped with a VR controller in their dominant hand, emulating a welding gun, and were tasked with welding a workpiece as accurately as possible within the VR environment. To enhance realism, welding gloves

were provided, and no time constraints were imposed. The welding task was visually represented by ink emitted from the weld gun tip upon contact with the workpiece, resulting in a visual weld line. The completed works were documented as screenshots for subsequent analysis.

Similar to Protocol A, subjects underwent quiet stance and kneeling with four TOIs in Protocol B: (i) TOI 5: Welding task in an LE without the exoskeleton; (ii) TOI 6: Welding task in an HE without the exoskeleton; (iii) TOI 7: Welding task in an LE with the exoskeleton; and (iv) TOI 8: Welding task in an HE with the exoskeleton. Participants were given test trials to get familiar with the welding setup and operation. Participants were allowed a 10-min rest period between each trial to prevent task-induced fatigue and ensure accurate task execution. In both Protocols A and B, the orders of the trials were randomized for evaluation purposes.

B. Data Collection and Processing Methods

During the experiments, the x - and y -axis were respectively defined as anterior-posterior (A-P), medial-lateral (M-L) directions. Fig. 2 illustrates two key measurements used in analysis to quantify movement variability and postural stability: the 95% acceleration ellipse area A_i^{Acc} and the 95% sway ellipse area A_i^{Sway} , $i = t, d$. A_i^{Acc} is calculated as the elliptical area that contains 95% of the acceleration variations (from IMU) in the A-P (\ddot{x}_i^m) and M-L (\ddot{y}_i^m) planes. It quantifies the variability in body accelerations and thus reflects the dynamic control and execution of movement. In contrast, A_i^{Sway} is obtained as the elliptical area that contains 95% COP data (from force plate) in the A-P (x_{CP}) and M-L (y_{CP}) directions. It represents the spatial variability of the COP movements, offering insights into the stability of postural equilibrium and the subject's ability to maintain or regain balance.

To evaluate welding task performance, digital image processing was used to analyze the images of the workpiece. Fig. 4 illustrates the extraction of correctly targeted welded area (A_t), outside area (A_o), unfinished area (A_u), and the total workpiece area (A_{wp}) to determine the accuracy of the welding efforts and to evaluate any unfinished segments. Three metrics were introduced to quantify the welding performance: accuracy, precision, and completion rate. Accuracy is defined as the ratio of the correctly welded area to the total workpiece area, i.e., $\frac{A_t}{A_{wp}}$. Precision measures the amount of welding that falls outside the targeted area, that is, $\frac{A_o}{A_w}$. Completion rate is assessed by the percentage of the

workpiece that has been welded, that is, $\frac{A_{wp} - A_u}{A_{wp}} \times 100\%$.

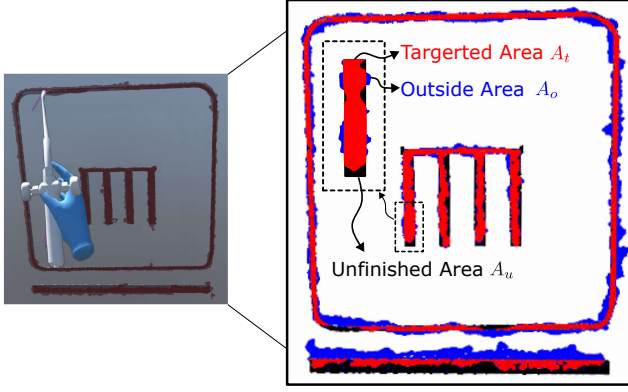


Fig. 4. Image processing method explanation for welding performance assessment on a virtual welding piece.

Subjective perceptions were also collected by pre- and post-experiment questionnaires (provided in the supplemental materials). Pre-experimentally, subjects' inherent fear responses were quantified using the James Geer Fear (JGF) questionnaire [32], and the Cohen Acrophobia (CA) questionnaire [33], aimed at understanding their reactions to heights. Both questionnaires used a five-point Likert scale [34]. A subsequent post-experiment questionnaire sought to elucidate subjects' experiences within the VR scene and their perceptions of the experimental procedures, aiming to refine and enhance the experimental design through iterative feedback. This dual approach, melding subjective feedback with objective data, provides a holistic understanding of the impact of experimental conditions on both the psychological and physiological dimensions of participant response.

IV. DATA ANALYSIS AND SIMULATION

Fig. 5 shows the overall procedure for IP-based data analysis and multi-task assessment. The GRF and COP data were first derived from the experimental and model simulation data. To obtain the frequency curve for the h_{IP} , the COP and GRF data in the A-P direction were first processed using a Hann window. The windowed signals were then bandpass filtered using a zero-lag, 2nd-order Butterworth filter into 38 non-overlapping frequency bands of 0.2 Hz width, centered from 0.5 to 7.9 Hz. Parsing the signals into these bands reveals an approximately linear relationship between the COP and GRF data within each frequency band. The reciprocal of the slope of this linear trace represents the h_{IP} for the corresponding frequency, as shown in (4) and (5).

Fig. 6 shows an example of the IP frequency curve normalized by $h_{COM} = z_i^m$. We focus on the crossover frequency (CF) of the IP height frequency curve with the COM height (i.e., ratio h_{IP}/h_{COM} at one), denoted as ω^{CF} , and the slope of the high-frequency asymptote (HFA), denoted as k^{HFA} . To determine and calculate k^{HFA} from the IP curves, an exponential fit was applied. For kneeling, the IP generally lies above the COM and it is challenging to define the CF and HFA in the same way as in quiet stance. To maintain

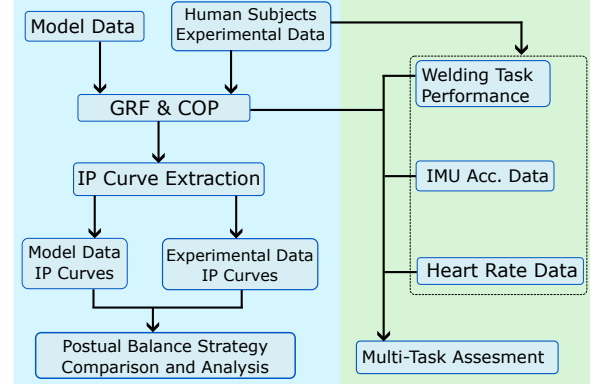


Fig. 5. Pipeline of intersection point height analysis and multi-task assessments.

consistency in the analysis of balance control strategies, we introduce the concept of virtual CF and HFA by normalizing the IP height as a fraction of the upright stance COM height; see Fig. 1(b).

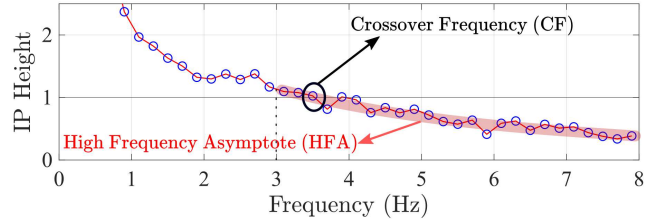


Fig. 6. Illustration of the crossover frequency ω^{CF} and the high-frequency asymptote (HFA) with slope k^{HFA} of the IP height frequency curve.

The IP frequency curves offer insights into human balance control strategies. At low frequencies, the IP height greater than the COM height indicates active neuromuscular engagement and high control effort to maintain balance. As the frequency increases, the IP curve decays, suggesting a transition from active to passive control strategies, characterized by ω^{CF} . The HFA slope k^{HFA} of the IP curve represents the passive control mechanism dominant at higher frequencies, reflecting the neuromechanical impedance of the joints.

After extracting the IP frequency curves, statistical analysis was conducted separately for the datasets of each subject group. The behavior of the IP curve was assessed through the quantification of three key parameters, namely, α_i , β_i , and σ_i , $i = t, d$, for stance and kneeling, respectively. The PSD of the COP data was also calculated to analyze the frequency content of the postural sway. The PSD quantifies the energy distribution of the COP signal across different frequency bands, allowing for the identification of dominant frequencies and their relative contributions to the overall postural control strategy. The heart rate data was incorporated into the multi-task assessment to examine the physiological responses of the subjects during the experiments. By integrating these diverse data sources, the study aims to provide a comprehensive understanding of the interplay between postural balance, exoskeleton assistance, task performance, and physiological responses in construction work.

We also conducted simulations to analyze the impact

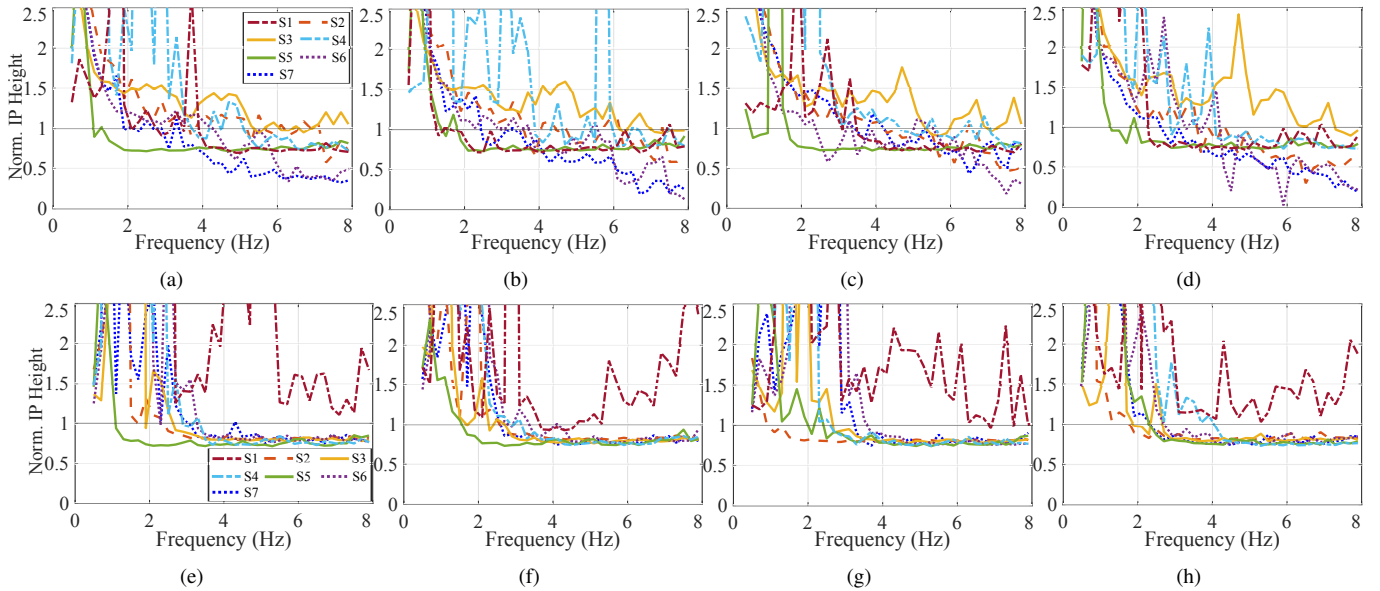


Fig. 7. Top row: Normalized stance balance task IP height-frequency curves for 7 subjects from TOI1-TOI4: (a) LE without exoskeleton; (b) HE without exoskeleton; (c) LE with exoskeleton; (d) HE with exoskeleton. Bottom row: Normalized stance welding task IP height-frequency curves for 7 subjects from TOI5-TOI8: (e) LE without exoskeleton; (f) HE without exoskeleton; (g) LE with exoskeleton; (h) HE with exoskeleton.

TABLE I
MODEL PARAMETERS FOR THE TIP AND DIP MODELS

Parameter	TIP			DIP	
	Link 1	Link 2	Link 3	Link 2	Link 3
m_i (kg)	6	14	48	20	42
l_i (m)	0.6	0.42	0.7	0.568	0.622
l_{ci} (m)	0.3	0.1	0.45	0.284	0.311
I_i (kgm^2)	0.264	0.1722	0.441	0.5	3.5

of various neural balance controller parameter sets on the IP height frequency curve. These simulations provided a controlled environment to investigate the complex interplay between various biomechanical and neurological factors contributing to human balance control. The simulation allowed for the exploration of a wide range of scenarios and conditions that may be difficult or impossible to test experimentally. To simulate and analyze the impact of control parameters on human balance strategies, the TIP and DIP models with the LQR-based neural controller with initial condition $\mathbf{x}(0) = \mathbf{0}$ to compute IP height frequency behaviors. Table I lists the parameter values for the models that were determined by typical human biomechanical data [35]. The simulation involved executing a series of trials to analyze the model's response under various conditions, each lasting 50 s with data sampled at a frequency of 100 Hz. To ensure robust statistical analysis, 30 trials were conducted for each parameter set.

V. RESULTS

A. Experimental Results

Figs. 7(a)-7(d) show the IP frequency curves for TOIs 1 to 4. The IP height magnitude is above the COM at lower frequencies, demonstrating greater control effort at these frequencies. The IP curve decays with increasing frequency,

indicating a reduced influence of active control. The IP curve also reaches an asymptote below the COM at high frequencies, suggesting a transition to passive control mechanisms. The spikes in the IP frequency curve indicate changes in balance strategy, which is direct effort of an individual attempting to stabilize the gait. On examining each individual's IP curve across TOIs, several observations are obtained. In the balance tests, for instance, subject S3 generated high frequency spikes in the IP curves when provided with exoskeleton assistance. The observation suggests a counter-intuitive perception of instability, causing the subjects to alter their balance strategies to maintain balance. Subject S6 also showed increased variation in the IP curve with the exoskeleton. On the other hand, presence of the exoskeleton reduced both high-frequency and high-magnitude spikes for S4. For S1, there were large spikes at for LE cases at low frequencies, while smaller spikes were observed for HE cases at high frequencies, indicating a shift in balance strategy on experiencing altered visual stimuli. It is evident that the interplay between HE and exoskeleton use did not uniformly impact all individuals; some subjects such as S5 and S7 maintained a consistent and stable balance strategy that remained unchanged across all balance TOIs, regardless of elevation or exoskeleton.

Figs. 7(e)-7(h) show the IP curves generated by subjects performing quiet stance while conducting welding tasks. The near absence of high frequency spikes is noted. Examination of these curves across individual subjects reveals that focusing on tasks (TOIs 5 to 8) generally enhances postural stability. When compared to the quiet balance, most subjects in kneeling gait exhibited smoother asymptotic behavior in the IP frequency response, which suggests a stable control strategy employed during the welding tasks. This improved stability can be a result of the subjects focusing on the welding task, permitting a stable balance strategy to be

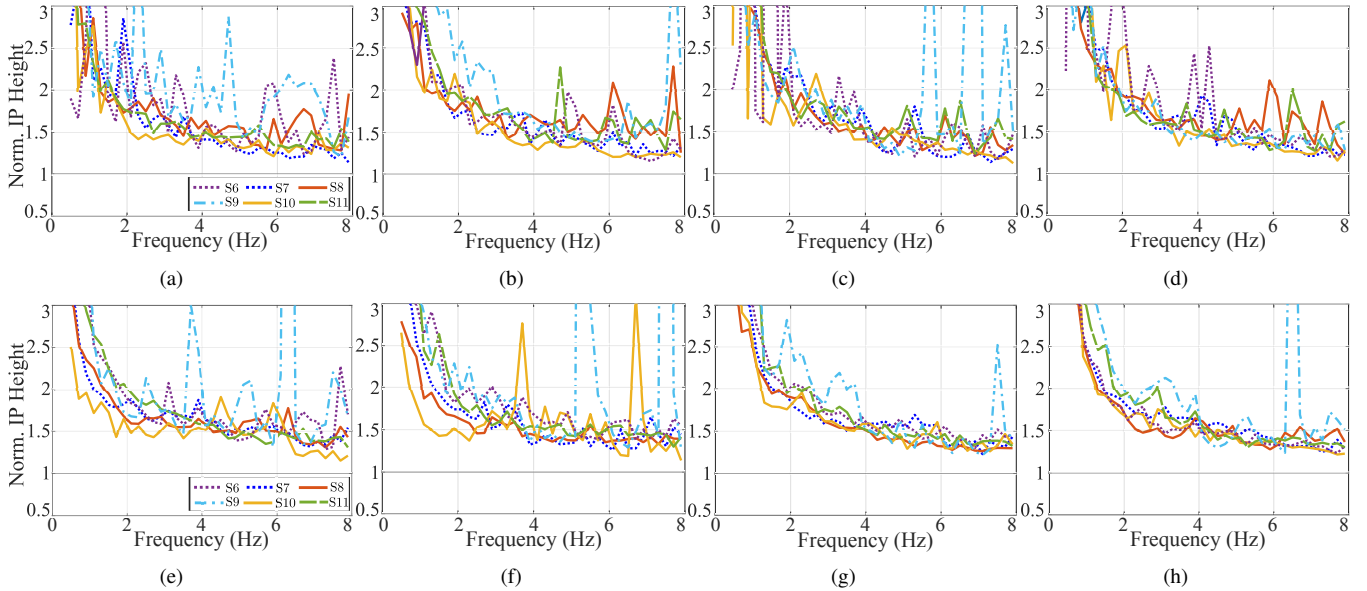


Fig. 8. Top row: Normalized kneeling balance task IP height-frequency curves for 6 subjects from TOI1-TOI4: (a) LE without exoskeleton; (b) HE without exoskeleton; (c) LE with exoskeleton; (d) HE with exoskeleton. Bottom row: Normalized Kneeling welding task IP height-frequency curves for 6 subjects from TOI5-TOI8: (a) LE without exoskeleton; (b) HE without exoskeleton; (c) LE with exoskeleton; (d) HE with exoskeleton.

instinctively chosen. An exception to this trend is observed in the case of subject S1, whose IP curve does not follow the typical characteristics expected of healthy human quiet stance. This can be attributed to the subject modifying their gait during task performance, transitioning from upright stance to a quarter-squat position. Thus, IP curves have the potential to discriminate between different types of gait, underscoring the advantages of exploring IP behavior in other common construction worker gaits.

Fig. 8 shows the IP height-frequency curves for the kneeling balance task and the kneeling welding task for 6 subjects. All kneeling curves are similar to the cases of quiet stance. The relative IP height in relation to the COM is overall higher in kneeling than in stance. The kneeling IP curves give insight into individual balance strategies in response to different testing stimuli. For the balance experiments, HE increased the magnitude of high frequency spikes in S8 and S11 and reduced the spikes in S6. The exoskeleton assistance reduced and increased high frequency spikes in LE balance tests for S8 and S9, respectively. When outfitted with the exoskeleton, S6, S7 and S10 show smoother IP curves during welding task performance. S9's balance strategy varied greatly across all TOIs with high frequency spikes in all cases except TOI 4. Overall, S6, S8 and S11 have smoother IP curves for TOIs 6 to 8 than those in TOIs 1 to 4.

TABLE II
MEAN IP DESCRIPTOR VALUES FOR ALL TOIS

TOI	1	2	3	4	5	6	7	8
$\bar{\omega}_t^{CF}$ (Hz)	3.2	3.6	3.2	3.4	2.2	2.7	2.4	2.6
$ \bar{k}_t^{HFA} $	0.103	0.068	0.117	0.010	0.018	0.022	0.012	0.018
$\bar{\omega}_d^{CF}$ (Hz)	3.9	3.9	4.1	4.1	5	3.9	5	4.2
$ \bar{k}_d^{HFA} $	0.023	0.014	0.014	0.043	0.018	0.052	0.047	0.033

Table II lists the mean values of ω_i^{CF} and k_i^{HFA} through

one-way ANOVA for all TOIs. Upon the introduction of the exoskeleton, there was a discernible decrease in the mean CF $\bar{\omega}_t^{CF}$ during the balance experiments, suggesting a shift in the balance control strategy employed by the subjects. The value of $\bar{\omega}_t^{CF}$ was also found to increase with the HE visuals. For the welding task scenario, overall $\bar{\omega}_t^{CF}$ is lower than that of the balance scenario, indicating the introduction of the task reduced balance control effort. While the combination of the exoskeleton and HE visuals lowered $\bar{\omega}_t^{CF}$ in the balancing experiments, performing welding tasks increased its value. The mean slope of the HFA $|\bar{k}_t^{HFA}|$ had a higher magnitude for the balance experiments than the welding task experiments. The condition of HE without exoskeleton had the lowest magnitude of $|\bar{k}_t^{HFA}|$, while LE with exoskeleton support had the highest $|\bar{k}_t^{HFA}|$ in balancing experiments. The vice-versa was true for the welding task performance experiments. The kneeling IP descriptors are also presented in Table. II. The value of $\bar{\omega}_d^{CF}$ does not vary with visual stimuli. It however increases with the exoskeleton assistance and welding task. The task performance increases the magnitude of $|\bar{k}_d^{HFA}|$ for HE without exoskeleton assistance and LE with exoskeleton assistance. For LE without exoskeleton support and HE with exoskeleton support, the values of $|\bar{k}_d^{HFA}|$ however decreased.

Fig. 9 shows the PSD curves under various test conditions. The figures compare the PSD results across the balance and welding task during stance and kneeling gaits. By examining the PSD plots, we can concisely analyze the postural sway behavior. For example, low postural sway is observed in welding task TOIs (asymptote begins around 0.4-0.6 Hz) compared to the balance TOIs (asymptote begins around 3-4 Hz), regardless of the gait performed. Stance overall has higher postural sway than kneeling gait as showcased by the PSD frequency curves located at higher frequencies. High-elevation visual feedback caused more postural sway during quiet stance than kneeling gait as seen by the higher

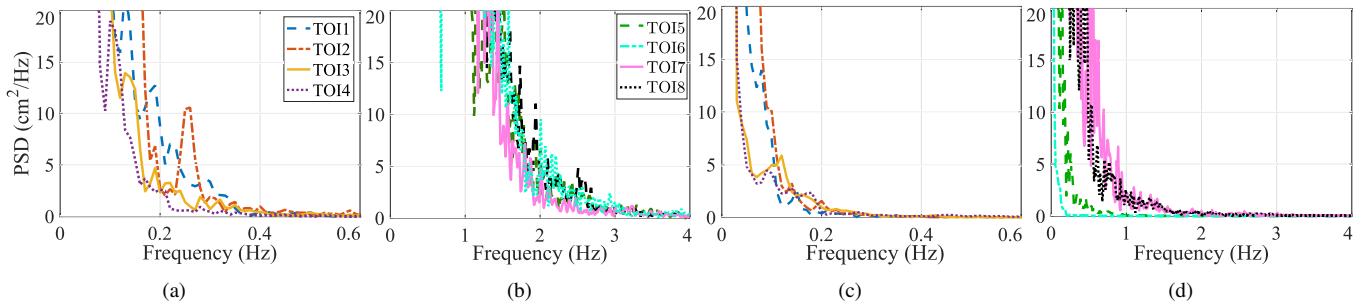


Fig. 9. Power spectral density of experimental COP results for (a) S4 under Protocol A with stance. (b) S4 under Protocol B with stance. (c) S7 under Protocol A with kneeling. (d) S7 under Protocol B with kneeling.

area under the curve. While the exoskeleton reduced the sway in most TOIs, it allows for increased sway in TOIs 7 and 8 during kneeling. As shown in Figs. 7 and 8, the IP methodology works to complement these observations by providing more detailed physiological and joint-level insights, as detailed in Section V-B.

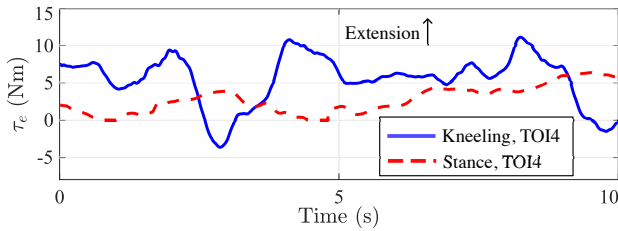


Fig. 10. An example of knee exoskeleton output torque τ_e for both stance and kneeling gaits in TOI 4.

Fig. 10 shows an example of assistive torque τ_e by the exoskeleton during a 10-s interval for both stance and kneeling gaits in TOI 4 from one subject. The stiffness-based controller during quiet stance generated extension torques and the gravity-compensating PD controller for kneeling demonstrated dynamic torque range. These torque outputs helped maintain the knee joint's desired position and stability. The effectiveness of the exoskeleton assistance in improving balance can be further observed through metrics such as the A_d^{Sway} and A_d^{Acc} , as shown in Fig. 11. The reduced ellipse areas in the presence of the exoskeleton, particularly during HE conditions and welding tasks, indicate that the device contributes to better postural stability and reduced body sway.

Fig. 12 further compares the sway acceleration ellipses and the postural sway ellipses for TOIs 2 and 4 experiments. The relatively larger ellipse areas for the kneeling gait compared to the stance gait, particularly under TOI 2, suggest that kneeling is inherently less stable than quiet stance. In the presence of higher cognitive load and visual disturbances, the exoskeleton provides significant support and stabilization during kneeling tasks, as evidenced by the reduced ellipse size compared to TOI 2. Table III lists the mean and standard deviation of A_t^{Acc} and A_t^{Sway} as quantitative assessments of postural stability. For quiet stance, there is a notable decrease in average A_t^{Sway} from TOI 1 and 2, signaling that subjects reduced their sway in response to visually induced stress. However, an increase of A_t^{Acc} suggests that the subjects responded with significant dynamic control to

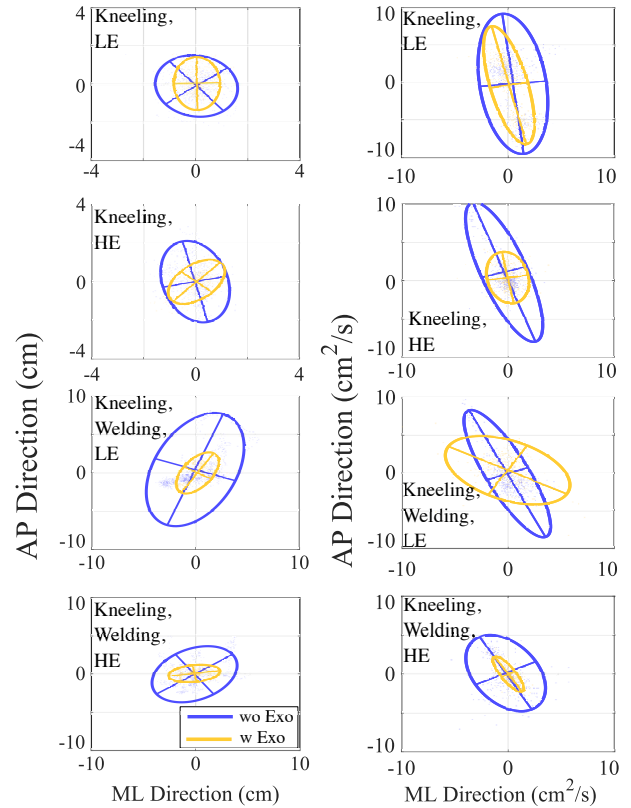


Fig. 11. A_d^{Sway} (left) and A_d^{Acc} (right) for a representative subject (S7) during kneeling experiments under different TOIs.

maintain this constrained posture. The stabilizing effect of the exoskeleton was evident in TOI 3, where reduced A_t^{Sway} and A_t^{Acc} correspond to a relaxed stance, while in TOI 4, with higher A_t^{Sway} but lower A_t^{Acc} values, indicates deliberate and controlled movements. Welding tasks, particularly TOI 6, show the largest A_t^{Acc} and A_t^{Sway} , indicating that engagement in the task necessitates broader movements. For kneeling condition, the overall A_d^{Acc} and A_d^{Sway} are smaller compared to the quiet stance condition, suggesting that the kneeling posture inherently constrains motion.

Fig. 13 shows the assessment of task performance through three metrics for the welding task across TOI 5 to 8. For quiet stance, it is observed that the incorporation of the exoskeleton in TOIs 7 and 8 correlates with improved accuracy and completion rate. The completion rate in HE conditions (i.e., TOI 8) is particularly enhanced with exoskeleton assistance,

TABLE III
MEAN SWAY AREA (CM²) AND SWAY ACCELERATION AREA (CM²/S)

TOI	1	2	3	4	5	6	7	8
A_t^{Acc}	30.1 ± 21.6	38.7 ± 24.9	17.2 ± 16.4	14.9 ± 9.9	248.2 ± 354.8	371.2 ± 562.5	275.8 ± 312.2	243.4 ± 259.6
A_t^{Sway}	43.3 ± 37.4	32.4 ± 21.2	15.3 ± 16.7	31.9 ± 28.6	109.3 ± 92.5	101.8 ± 68.2	134.5 ± 107.9	101.4 ± 77.4
A_d^{Acc}	19.9 ± 21.7	9.4 ± 2.7	6.1 ± 6.0	10.9 ± 7.7	25.6 ± 19.8	35.4 ± 29.2	20.5 ± 14.7	14.5 ± 4.9
A_d^{Sway}	2.6 ± 2.8	2.9 ± 3.4	1.5 ± 1.3	1.8 ± 1.2	14.4 ± 9.8	24.7 ± 23.7	18.4 ± 20.3	21.1 ± 15.5

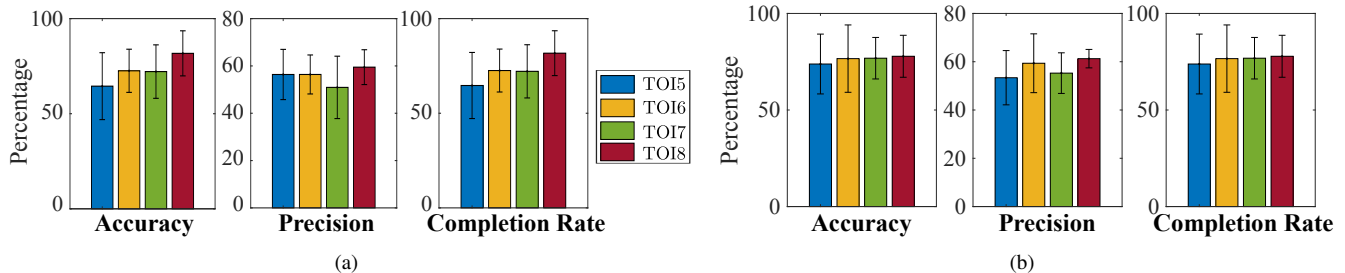


Fig. 13. Performance metrics for the virtual welding task across four TOIs for (a) quiet stance and (b) kneeling gaits.

TABLE V
SUBJECT QUESTIONNAIRE RESULTS

Subject ID		S1	S2	S3	S4	S5	S6	S7	S8	S9	S10	S11
JGF Quest.	Suscept. fear	63	123	93	98	65	112	125	85	61	89	132
CA Quest.	Fear Heights	22	56	40	40	27	53	54	33	48	45	60
	Avoid. HE	22	36	26	28	23	36	34	27	49	36	37
Cog. Load	Stressful	HE+Exo	HE+Exo	HE	HE	HE	HE/HE+Exo	HE	HE	HE	HE	HE
	Relaxed	LE	LE+Exo	LE+Exo	LE	LE	LE/LE+Exo	LE+Exo	LE+Exo	LE+Exo	LE+Exo	LE
Task Perf.	Most Focus	HE	HE+Exo	HE+Exo	LE+Exo	HE+Exo	LE/HE+Exo	HE+Exo	LE+Exo	LE+Exo	LE+Exo	LE+Exo
	Least Focus	LE+Exo	LE	HE	HE	HE	LE+Exo/LE	LE	HE	HE	HE	HE

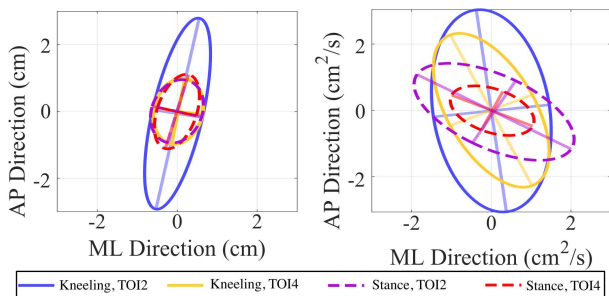


Fig. 12. Comparison of A_t^{Sway} (left) and A_t^{Acc} (right) between kneeling and stance gaits under TOIs 2 and 4.

whereas precision appears to be less influenced by the elevation or the presence of the exoskeleton. The kneeling gait exhibits a similar trend in task performance metrics. The use of the exoskeleton in TOIs 7 and 8 under kneeling conditions also leads to increased accuracy and completion rate compared to TOIs 5 and 6 without exoskeleton assistance. This finding suggests that the exoskeleton's benefits extend beyond a quiet stance and can effectively support task execution in kneeling postures as well. However, it is worth noting that the overall accuracy and completion rate values for kneeling are slightly lower than those for quiet stance across all TOIs. This difference may be attributed to the inherent challenges associated with maintaining balance

and performing tasks in a kneeling posture.

Fig. 14 shows the heart rate data collected during the welding tasks for both gaits. During quiet stance, the heart rate increased from LE to HE suggests a progressive elevation in stress levels, with the highest median heart rate recorded during the HE tasks, regardless of exoskeleton usage. This incremental pattern reflects the physiological demands imposed by elevation changes and the complexity of tasks performed under such conditions. With the introduction of the knee exoskeleton, subjects experienced a reduction in stress levels during tasks at both LE and HE. During kneeling gaits, although the application of the exoskeleton reduced human effort and lowered the heart rate, the heart rate was generally higher compared to a quiet stance. Table IV lists the average heart rates from some subjects for TOI 5 to 8. The data reveal minimal fluctuations in heart rate among most subjects across different TOIs, suggesting that the welding task may serve as a focal stimulus, concentrating the participants' attention and thereby stabilizing physiological responses [23]. Subjects S2, S3, and S5 demonstrated notable variations in average heart rate upon the integration of the exoskeleton into the task during stance gait. Similar trends are observed during kneeling gaits, where most subjects experienced a reduction in heart rates with exoskeleton assistance while performing welding tasks.

Table V summarizes the results from the subjects' ques-

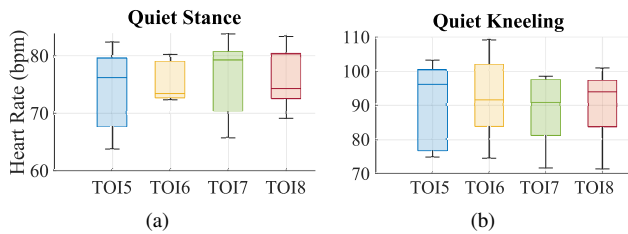


Fig. 14. Heart rate comparison for the virtual welding task across four TOIs during (a) quiet stance and (b) kneeling gaits.

TABLE IV
MEAN HEART RATE DATA (IN BPM)

Quiet Stance/Kneeling				
Subject	TOI5	TOI6	TOI7	TOI8
S1 / S8	79.4/100.4	79.5/87.0	79.7/98.5	83.4/97.3
S2 / S9	66.0/103.3	65.7/96.6	73.0/97.5	74.4/92.7
S3 / S10	82.4/76.8	81.1/84.1	73.6/81.4	72.6/83.8
S4 / S11	79.6/74.9	83.8/74.5	80.3/71.7	78.2/71.4
S5	63.8/—	69.6/—	72.4/—	72.8/—
S6	73.0/95.8	72.5/109.2	72.8/87.0	69.1/95.4
S7	76.3/96.3	79.3/102.0	77.0/95.2	81.1/101.0

tionnaire feedback. The data indicates a wide range of susceptibility to fear and acrophobia across all subjects for both quiet stance and kneeling gaits. In quiet stance experiments, subjects S2 and S7 showed the highest levels of susceptibility to fear and acrophobia, whereas S1 displayed the lowest. For kneeling tests, S11 exhibited the highest susceptibility to fear and S9 had the lowest. Cognitive loading was reported to be higher during tasks at HE for most subjects than that at LE in both stance and kneeling experiments. However, subjects S1 and S2 in quiet stance and S6 in kneeling experiments reported high cognitive load with the exoskeletons at HE. When considering task performance, subjects generally focused best on the addition of the exoskeletons, while their focus was compromised without the exoskeletons. This trend was observed in both gaits experiments, suggesting that the exoskeleton may offer a psychological benefit in high-stress situations, regardless of the working posture.

All subjects reported feeling tense during HE scenarios and calm during low elevation scenarios, with varied responses to the presence of the exoskeleton. However, it should be noted that the subjects' perception of focus and relaxation does not always equate to good postural balance and balancing choices. Stressful situations, such as focusing on welding, can lead to instinctive balance strategies being chosen, resulting in better balance. Perturbations under stressful situations can cause posture to rapidly become unstable. In the stance experiments, subjects S1 and S2 expressed an increase in stability and balance when utilizing the exoskeleton. In contrast, S7 experienced a restriction in mobility due to the exoskeleton. Meanwhile, S5 noticed a marginal benefit, and S6 found that the exoskeletons helped maintain position during the task. The responses to height exposure were equally varied. Most subjects consistently described the HE environment as

highly realistic and fear-inducing. Interestingly, all participants in the kneeling experiments reported enhanced stability and reduced effort in maintaining balance when using the exoskeletons.

B. Simulation Results

The best-fit parameters were derived by varying the parameter sets to obtain frequency behavior matching the observed frequency behavior of humans during quiet stance across various TOIs. Fig. 15 demonstrates an example of exponential fitting on experimental stance and kneeling IP curves. Table VI lists the resulting best-fit parameter sets that quantify the favored balance strategy corresponding to each TOI. The simulated IP curve that generates the minimum error in comparison to the exponentially fitted experimental IP curve is identified.

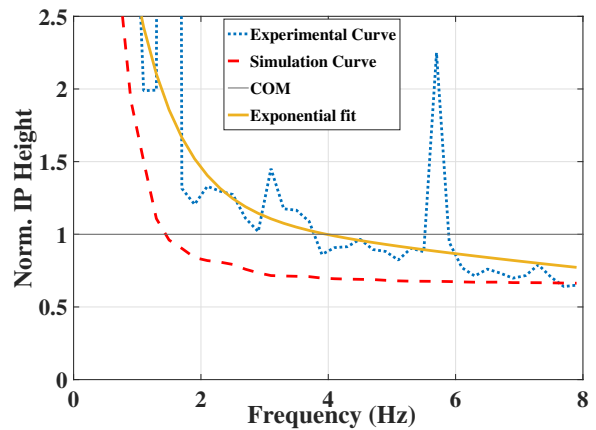


Fig. 15. Comparison among the experiment, simulated, and exponentially fitted IP curves for both gaits.

TABLE VI
BEST-FIT LQR CONTROLLER PARAMETERS FOR QUIET STANCE TOI

TOI	Case	α	β_1	β_2	β_3	σ_1	σ_2	σ_3
1	LE	10^6	0.2	0.1	0.3	1	1	1
2	HE	10^{10}	0.3	0.1	33.3	1	1	1
3	LE+Exo	10^6	0.2	0.1	0.3	0.7	0.3	1
4	HE+Exo	10^6	0.2	0.1	0.3	0.7	0.3	1
5	LE Weld	10^{10}	0.2	0.1	0.3	1	1	1
6	HE Weld	10^{10}	0.2	0.1	0.3	1	0.7	0.3
7	LE+Exo Weld	10	0.3	0.1	33.3	1	1	1
8	HE+Exo Weld	10^{10}	0.2	0.1	0.3	1	1	1

Examining the variations in α values reveals a characteristic for minimal control effort. A high α magnitude signifies a minimal control effort and is generally chosen by humans during quiet stance, yet this tendency differs across different TOIs. For the balancing experiments, all cases had a high magnitude of α , with TOI 2 utilizing the lowest control effort. The same results were observed from the task performance scenarios TOIs 5, 6, and 8, while TOI 7 had a lower magnitude of $\alpha = 10$. The low value of α implies that a non-minimal effort control strategy was unexpectedly chosen to balance. This anomaly potentially suggests that the subjects

could have altered their balance strategies to adapt to the exoskeleton in the presence of non-threatening visuals, rather than passively rely on the extra support it provides. For the rest of the welding cases, α value (i.e., 10^{10}) is high, which implies that the welder's main focus on precision during the welding task caused them to use a minimal effort balance strategy.

The balance strategies were further refined by the choice of joint strategy, as determined by the β values. Across all TOIs, it was found that $\beta_2 < \beta_1 < \beta_3$, which suggests employing hip strategy is penalized compared to employing ankle-knee strategies. TOIs 2 and 7 have higher β_3 values, with subjects favoring the ankle-knee strategy heavily over the hip strategy to balance. The preference for the ankle-knee strategy in TOI 2 can be the consequence of the destabilizing visuals, with the subjects attempting to keep their head, the visual source of the body, stable and upright. For potentially similar reasons, TOI 6 shows relatively higher noise values at the ankle (σ_1) and knee joints (σ_2) than at the hip joint (σ_3). For TOI 7, the high effort control strategy suggests that the ankle-knee strategy chosen, while intentional, required much effort to maintain balance. The neuromechanical noise at the knee joint is lower with the presence of the exoskeleton for the stance case (TOIs 3 and 4). On introducing the VR task scenario, the neuromechanical noise experienced is similar at all joints with the exoskeleton. A similar balance strategy is used for both TOI 3 and 4, thus exhibiting reduced influence of visual stimuli on balance with the exoskeleton in the absence of task performance.

VI. DISCUSSION

The balance strategies discerned from IP curve analyses suggest active neuromuscular engagement at lower frequencies and a transition to passive control strategies at higher frequencies, modulated by the knee exoskeleton. The decrease in mean CF $\bar{\omega}^{\text{CF}}$ with exoskeleton application implies an adaptive response in the human balance control system, possibly reflecting augmented stability. The consistency in the mean HFA slope \bar{k}^{HFA} across TOIs with exoskeleton intervention indicates uniform neuromechanical impedance on the joints, with the high slope interpreted as an increment in neuromechanical noise and a strategic shift in balance at high frequencies. The altered strategy can be a consequence of the individuals' effort to recalibrate their balance strategy to accommodate the exoskeleton during task execution (e.g., TOI 7), as opposed to being passively supported in a static posture (TOI 8). The results from Tables II align with the notion in [27] that while exoskeletons can enhance postural control, their impact on the neuromechanical behavior of the body is predictable and can be characterized by specific frequency-domain features of the IP curve. These insights are pivotal for optimizing the design of exoskeletons to harmonize with the body's natural balance strategies. By observing the parameter α , it was also found that kneeling balance control requires much higher effort than during stance to maintain postural stability.

As shown in Fig. 7, the introduction of the welding task increased presence of low frequency spikes in the rest of the subjects' IP curves. Low frequency spikes reflect proactive intentional efforts to change the balance strategy rather than reactionary attempts to stabilize stance in response to environmental perturbations. While low frequency spikes reduced with exoskeleton assistance for S5, they increased for S6 for both balance and task performance TOIs. The subject specific insights drawn from the IP analysis are valuable in identifying subjects who may be susceptible to destabilization due to specific task scenarios, thereby informing necessary measures to mitigate the risk of injury.

Task performance assessments reveal the exoskeleton's potential to alleviate the cognitive and physical loads on the subject in the presence of higher cognitive load and visual disturbances in construction. The comparative analysis between quiet stance and kneeling emphasizes the need for targeted interventions and training programs addressing specific challenges associated with different working postures. The increase in heart rate during kneeling can be attributed to greater muscle activation, reduced venous return, and psychological stress [36], [37]. The combination of physiological metrics permits a distinction between physical and cognitive stressors, highlighting the complexity of the exoskeleton's effectiveness in high-stress tasks. The consistency in precision values suggest that the exoskeleton primarily aids in postural stability and task completion rather than fine motor control.

By considering the GRF intersection point, the IP method provides a comprehensive assessment of the worker's postural control mechanisms. This approach is particularly valuable in the context of construction work, where workers are exposed to a wide range of environmental conditions, such as elevated work surfaces and unstable footing. By analyzing the frequency characteristics of the IP heights, researchers and safety professionals can gain insights into how workers adapt their balance strategies in response to different work scenarios. It is noteworthy that only a specific subset of β value sets could effectively describe the IP characteristics across various TOIs. The knee joint strategies play a crucial and non-trivial role in maintaining balance, highlighting the importance of considering knee joint control when designing balance-assistive devices or developing balance training programs for construction workers.

In contrast to the previous work in [6], which focused on a single-link inverted pendulum model, the current study employs a more comprehensive approach to capture the complexity of balance control in real-world construction scenarios. The research work in [6] employed the PSD analysis to examine postural balance. This metric, as demonstrated in this study, can providing valuable insights into the dominant frequencies of sway. However, PSD analysis alone cannot provide a comprehensive understanding of the underlying neuromechanical strategies employed by individuals to maintain balance (see Fig. 9), as it does not capture the spatial organization, coordination, or phase relationships between different body segments. Using the IP, multi-link inverted pendulum models and the LQR controller, the current work

analyzed the model's response to various conditions and the interpretation of the results in terms of physiological and biomechanical implications. The LQR controller aligns with the hypothesis that the human neural system employs an optimal control strategy to maintain balance [25], [26] and has been supported by numerous studies (e.g., [38]).

Despite the reported benefits in terms of stability and balance, some subjects expressed that wearing the knee exoskeleton was less comfortable during kneeling compared to the stance posture. This disparity in comfort levels may be attributed to the unique biomechanical demands and joint configurations associated with kneeling. These observations underscore the importance of considering posture-specific design factors and adaptability when developing wearable exoskeletons for construction workers. There are some other limitations to consider for future research directions. First, although the VR environment allows for a controlled and safe investigation of various scenarios, future work should further validate these findings in real-world construction settings. Second, we recruited young and healthy subjects for this study and we should expand the subject pool to include experienced construction workers of all ages to provide a comprehensive evaluation of the exoskeletons' impact on balance and performance.

VII. CONCLUSIONS

This study provided insights into the influence of lower-limb joints on neural balance control in quiet stance and kneeling gaits in construction. The use of triple- and double-link inverted pendulum models, coupled with the intersection point height frequency analysis and the linear quadratic controller, allowed for a comprehensive evaluation of the balance strategies of the subject at the joint level. The integration of VR/MR tools to simulate elevated environments and welding tasks enabled the assessment of the impact of elevation and wearable knee exoskeletons on postural balance and task performance. The multi-subject experiment results highlight the critical role of knee joint strategies in maintaining postural stability and the potential of wearable exoskeletons in enhancing worker safety and performance in hazardous construction environments. The evaluation pipeline developed in this study can be further applied to assess the potential of wearable assistive devices across diverse occupational work settings.

REFERENCES

- [1] K. T. Palmer, "Occupational activities and osteoarthritis of the knee," *British Med. Bullet.*, vol. 102, no. 1, pp. 147–170, 2012.
- [2] D. A. Winter, A. E. Patla, F. Prince, M. Ishac, and K. Giello-Perczak, "Stiffness control of balance in quiet standing," *J. Neurophysiol.*, vol. 80, pp. 1211–1221, 1998.
- [3] J. L. Allen and L. H. Ting, "Why is neuromechanical modeling of balance and locomotion so hard?" in *Neuromech. Modeling of Posture and Locomotion*, B. I. Prilutsky and D. H. Edwards, Eds. New York: Springer, 2016, pp. 197–223.
- [4] W. L. Boehm, K. M. Nichols, and K. G. Gruben, "Frequency-dependent contributions of sagittal-plane foot force to upright human standing," *J. Biomech.*, vol. 83, pp. 305–309, 2019.
- [5] D. A. Winter, A. E. Patla, S. Rietydyk, and M. G. Ishac, "Ankle muscle stiffness in the control of balance during quiet standing," *J. Neurophysiol.*, vol. 85, no. 6, pp. 2630–2633, 2001.
- [6] S. Chen, Y. Yu, C. Di, M. Trkov, J. Gong, and J. Yi, "Postural balance of kneeling gaits on inclined and elevated surface for construction workers," in *Proc. IEEE Conf. Automat. Sci. Eng.*, Lyon, France, 2021, pp. 753–758.
- [7] A. Yamamoto, S. Sasagawa, N. Oba, and K. Nakazawa, "Behavioral effect of knee joint motion on body's center of mass during human quiet standing," *Gait Posture*, vol. 41, pp. 291–294, 2015.
- [8] M. Günther, S. Grimmer, T. Siebert, and R. Blickhan, "All leg joints contribute to quiet human stance: a mechanical analysis," *J. Biomech.*, vol. 42, no. 16, pp. 2739–2746, 2009.
- [9] R. A. Mezzarane and A. F. Kohn, "Postural control during kneeling," *Exp. Brain Res.*, vol. 187, pp. 395–405, 2008.
- [10] K. G. Gruben and W. L. Boehm, "Mechanical interaction of center of pressure and force direction in the upright human," *J. Biomech.*, vol. 45, no. 9, pp. 1661–1665, 2012.
- [11] K. Shiozawa, J. Lee, M. Russo, D. Sternad, and N. Hogan, "Frequency-dependent force direction elucidates neural control of balance," *J. Neuroeng. Rehabil.*, vol. 18, no. 1, pp. 1–12, 2021.
- [12] A. Bhattacharya, P. Succop, L. Kincl, M. L. Lu, and A. Bagchee, "Postural stability during task performance on elevated and/or inclined surfaces," *Occup. Ergon.*, vol. 3, pp. 83–97, 2002/2003.
- [13] C. C. Boffino, C. S. C. De Sá, C. Gorenstein, R. G. Brown, L. F. Basile, and R. T. Ramos, "Fear of heights: Cognitive performance and postural control," *Europ. Arch. Psychiatry Clin. Neurosci.*, vol. 259, pp. 114–119, 2009.
- [14] M. Habibnezhad, J. Puckett, M. S. Fardhosseini, H. Jebelli, T. Stentz, and L. A. Pratama, "Experiencing extreme height for the first time: The influence of height, self-judgment of fear and a moving structural beam on the heart rate and postural sway during the quiet stance," *arXiv preprint arXiv:1906.08682*, 2019.
- [15] X. Xing, H. Li, J. Li, B. Zhong, H. Luo, and M. Skitmore, "A multicomponent and neurophysiological intervention for the emotional and mental states of high-altitude construction workers," *Automat. Constr.*, vol. 105, 2019, article 102836.
- [16] H. Luo, X. Wang, M. Fan, L. Deng, C. Jian, M. Wei, and J. Luo, "The effect of visual stimuli on stability and complexity of postural control," *Fronti. Neurology*, vol. 9, 2018, article 48.
- [17] I. Awolusi, E. Marks, and M. Hallowell, "Wearable technology for personalized construction safety monitoring and trending: Review of applicable devices," *Automat. Constr.*, vol. 85, pp. 96–106, 2018.
- [18] M. Trkov, K. Chen, J. Yi, and T. Liu, "Inertial sensor-based slip detection in human walking," *IEEE Trans. Automat. Sci. Eng.*, vol. 17, no. 1, pp. 348–360, 2020.
- [19] S. Chen, D. Stevenson, S. Yu, M. Mioskowska, J. Yi, H. Su, and M. Trkov, "Wearable knee assistive devices for kneeling tasks in construction," *IEEE/ASME Trans. Mechatronics*, vol. 26, no. 4, pp. 1989–1996, 2021.
- [20] C. Zhu and J. Yi, "Knee exoskeleton-enabled balance control of human walking gait with unexpected foot slip," *IEEE Robot. Automat. Lett.*, vol. 8, no. 11, pp. 7751–7758, 2023.
- [21] P. I. Simeonov, H. Hsiao, B. W. Dotson, and D. E. Ammons, "Height effects in real and virtual environments," *Human Factors*, vol. 47, no. 2, pp. 430–438, 2005.
- [22] Y. Shi, J. Du, C. R. Ahn, and E. Ragan, "Impact assessment of reinforced learning methods on construction workers' fall risk behavior using virtual reality," *Automat. Constr.*, vol. 104, pp. 197–214, 2019.
- [23] M. Habibnezhad, J. Puckett, H. Jebelli, A. Karji, M. S. Fardhosseini, and S. Asadi, "Neurophysiological testing for assessing construction workers' task performance at virtual height," *Automat. Constr.*, vol. 113, 2020, article 103143.
- [24] X. Li, W. Yi, H.-L. Chi, X. Wang, and A. P. Chan, "A critical review of virtual and augmented reality (VR/AR) applications in construction safety," *Automat. Constr.*, vol. 86, pp. 150–162, 2018.
- [25] A. D. Kuo, "An optimal control model for analyzing human postural balance," *IEEE Trans. Biomed. Eng.*, vol. 42, no. 1, pp. 87–101, 1995.
- [26] H. van der Kooij, R. Jacob, B. Koopman, and H. Grootenboer, "A multisensory integration model of human stance control," *Biol. Cybern.*, vol. 80, pp. 299–308, 1999.
- [27] G. Sreenivasan, C. Zhu, and J. Yi, "Neural balance control of human quiet stance in construction tasks," in *Proc. IEEE Conf. Automat. Sci. Eng.*, Auckland, New Zealand, 2023.

- [28] G. Sreenivasan, "Wearable knee exoskeleton-assisted postural balance enhancement for industrial workers," Master's thesis, Dept. of Elect. and Comp. Eng., Rutgers Univ., New Brunswick, NJ, 2023.
- [29] S. Yu, T.-H. Huang, X. Yang, C. Jiao, J. Yang, H. Hu, S. Zhang, Y. Chen, J. Yi, and H. Su, "Quasi-direct drive actuation for a lightweight hip exoskeleton with high backdrivability and high bandwidth," *IEEE/ASME Trans. Mechatronics*, vol. 25, no. 4, pp. 1794–1802, 2020.
- [30] G. Sreenivasan, C. Zhu, and J. Yi, "Knee stiffness in assistive device control at quiet stance: A preliminary study," *IFAC PapersOnLine*, vol. 56, no. 3, pp. 163–168, 2023.
- [31] C. Zhu, F. Han, and J. Yi, "Wearable sensing and knee exoskeleton control for awkward gaits assistance," in *Proc. IEEE Conf. Automat. Sci. Eng.*, Mexico City, Mexico, 2022, pp. 2393–2398.
- [32] J. H. Geer, "The development of a scale to measure fear," *Behav. Res. Therapy*, vol. 3, no. 1, pp. 45–53, 1965.
- [33] D. C. Cohen, "Comparison of self-report and overt-behavioral procedures for assessing acrophobia," *Behav. Therapy*, vol. 8, no. 1, pp. 17–23, 1977.
- [34] A. Joshi, S. Kale, S. Chandel, and D. K. Pal, "Likert scale: Explored and explained," *British J. Appl. Sci. & Technol.*, vol. 7, no. 4, pp. 396–403, 2015.
- [35] D. A. Winter, *Biomechanics and Motor Control of Human Movement*, 4th ed. New York, NY: John Wiley & Sons Inc., 2009.
- [36] K. M. Gallagher, T. Campbell, and J. P. Callaghan, "The influence of a seated break on prolonged standing induced low back pain development," *Ergonomics*, vol. 57, no. 4, pp. 555–562, 2014.
- [37] F. Gao, Y. Ren, E. J. Roth, R. Harvey, and L.-Q. Zhang, "Effects of repeated ankle stretching on calf muscle–tendon and ankle biomechanical properties in stroke survivors," *Curr. Biol.*, vol. 26, no. 5, pp. 516–522, 2011.
- [38] S. H. Scott, "Optimal feedback control and the neural basis of volitional motor control," *Nature Rev. Neurosci.*, vol. 5, no. 7, pp. 532–545, 2004.